Chapter 2

Mono Lacunary Silicotungstate (SiW_{11}) anchored to MCM-48:

Synthesis, Characterization and Esterification as well as Acetalization reactions

On similar lines to parent POMs, LPOMs also possess potential importance in the field of catalysis due to their structural diversities and electronic properties [1]. In this regard, the mono lacunary silicotungstate (SiW_{11}) based materials have also been explored as heterogeneous catalysts for the various transformations.

A literature survey shows that two decades past in 2002, Hu et al. prepared composite films of SiW_{11} with silica (SiO_2) and applied them for the photodegradation of aqueous formic acid [2] and malic acid [3]. Yang et al. (2011) showed the synthesis of SiW_{11} grafted mesoporous hybrid silica, SiW_{11}/MHS and exhibited stable, reversible photochromic properties based on UV irradiation [4]. In 2013, Cunha-Silva et al. reported the synthesis of potassium salts of the SiW_{11}, incorporated into the porous Metal-Organic Framework MIL-101(Cr) and used for the oxidation of cis-cyclooctene, geraniol and R-(+)-limonene [5]. Xue et al. in 2017 synthesized Cu and Fe doped SiW_{11} and assessed its catalytic activity in the oxidation of benzyl alcohol using hydrogen peroxide [6]. In 2010 Patel et. al reported synthesis of SiW_{11} supported onto zirconia and its use for esterification of sec-butanol and isobutanol with acetic acid [7]. The same group in 2013, 2014 and 2019 developed supported catalysts based on SiW_{11}, MCM-41 and Hβ. They investigated the catalytic acetalization, esterification and transesterification reactions for biodiesel synthesis [8,9].

From the above literature survey as well as the survey mentioned in General Introduction, it was observed that studies majorly report oxidation reactions. While for the esterification of levulinic acid and succinic acid as well as acetalization of glycerol, there are no reports available on mono lacunary silicotungstate based heterogeneous catalyst.

In addition, the spectacular catalytic activity of SiW_{12}/nMCM-48 for the said transformations of bioplatform molecules inspired us to design another catalyst i.e., mono lacunary silicotungstate (SiW_{11}) anchored to nMCM-48, for identical applications. Furthermore, it is expected that the acidity of lacunary POMs is less as compared to the parent POMs [10], therefore it was a study of interest to investigate the influence of addenda atom on the catalytic activity.

In this regard, the present chapter describes the synthesis of mono lacunary silicotungstate (SiW_{11}) and the catalyst, mono lacunary silicotungstate anchored to nMCM-48 (SiW_{11}/nMCM-48). The synthesized materials were characterized for acidity measurement, BET surface area measurements, elemental analysis (EDS), TGA, FT-IR, Powder XRD, ^{29}Si MAS NMR and TEM. The catalytic efficiency of the catalyst was investigated for the esterification of levulinic and succinic acid with n-butanol as well as the acetalization reaction of glycerol with furfural. A detailed optimization study for all the reactions was carried out by keeping the experiments in varying reaction parameters, such as mole ratio of reactants, catalyst amount, reaction temperature and time. To identify the sustainable nature of the catalyst, recycling experiments, as well as characterization of regenerated catalyst, were also carried out. Correspondingly, the activation energy for each reaction was determined by conducting kinetic experiments at different temperatures and time. Further, a mechanism for each system was also proposed.

EXPERIMENTAL

Materials

All the chemicals of A. R. grade were used. Sodium tungstate dihydrate, sodium silicate, nitric acid (65%), acetone, liquor ammonia, tetraethylorthosilicate (TEOS), levulinic acid, succinic acid, glycerol, furfural, n-butanol, ethanol, methanol, 2-propanol and dichloromethane were used as received from Merck.

Synthesis of support

The synthesis of support, nMCM-48 was carried out by the method as discussed in Part A Chapter-1 [Page 68-69].

Synthesis of sodium salt of mono lacunary silicotungstate ($Na_8SiW_{11}O_{39}$, SiW_{11})

Sodium salt of mono lacunary silicotungstate ($Na_8SiW_{11}O_{39}$, later SiW_{11}) was synthesized by the method previously reported by us [7]. 7.2 g (0.22 mol) sodium tungstate and 0.56 g (0.02 mol) sodium silicate were dissolved in 150 - 200 mL of distilled water and allowed to heat at 80-90 °C. The pH was adjusted to 4.8 - 5.2 by dropwise addition of (1:1) concentrated nitric acid solution and the volume was reduced to half by evaporation. Through liquid-liquid extraction with 80–100 mL of acetone, the heteropoly anion was separated and the extraction was repeated until the acetone extract showed the absence of NO^{3-} ions (ferrous sulfate test). The oily layer of sodium salt was triturated using fresh acetone and dried in the air. The resulting material is designated as SiW_{11}. A schematic representation of the procedure is shown in Scheme 1.

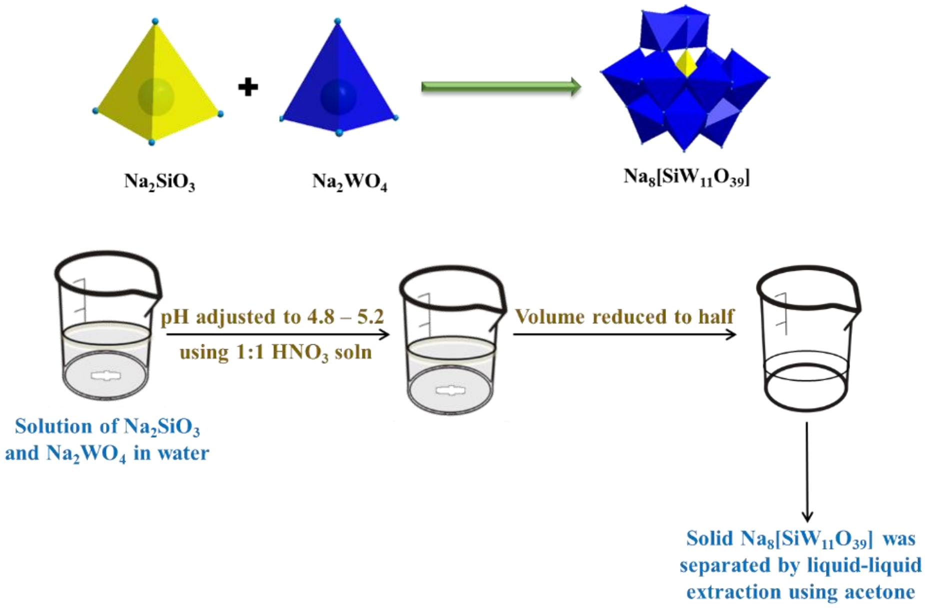

Scheme 1 Synthesis of SiW_{11}

Synthesis of catalyst, mono lacunary silicotungstate anchored to nMCM-48 (SiW_{11}/nMCM-48)

A series of catalysts with different loading amounts of SiW_{11}, from 10 to 40% were prepared by the wet impregnation method. In an aqueous solution of SiW_{11} (0.1 g/10 mL to 0.4/40 mL in double distilled water), 1 g of the catalyst was suspended and the solvent was evaporated at 100 °C. It was further dried for 10 h. The obtained solid materials were treated with 0.1 N HCl solution to convert the Na^+ ions into H^+ ions and dried at the same temperature. The resulting materials were designated as $(SiW_{11})_1$/nMCM-48, $(SiW_{11})_2$/nMCM-48, $(SiW_{11})_3$/nMCM-48 and $(SiW_{11})_4$/nMCM-48, respectively. A schematic representation of the procedure is shown in Scheme 2.

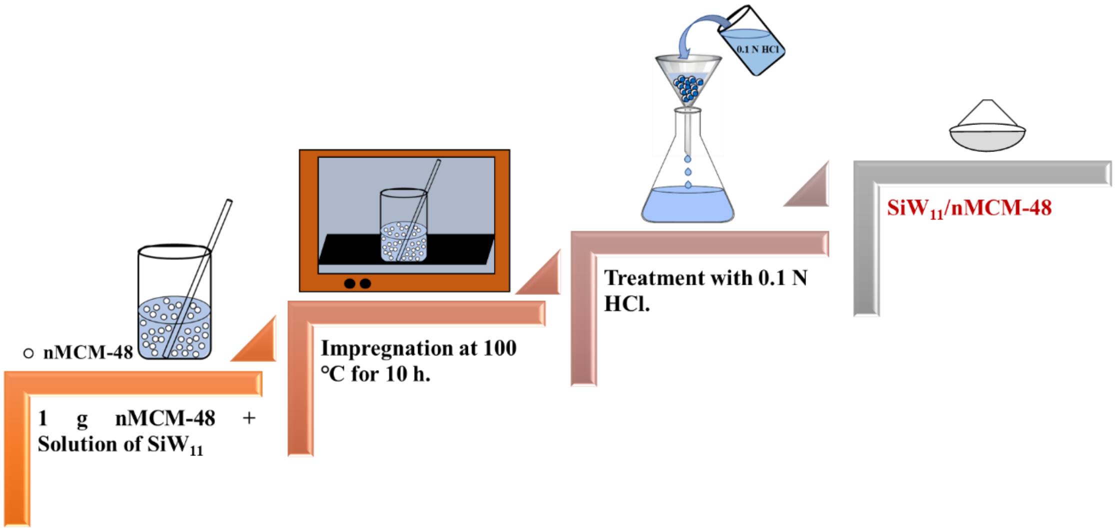

Scheme 2 Synthesis of SiW_{11}/nMCM-48

Characterization

Characterization of SiW_{11}, as well as SiW_{11}/nMCM-48, was carried out by the same physicochemical techniques as mentioned in General Introduction [Page 41-46]

Catalytic activity

The esterification reaction of levulinic acid and succinic acid as well as the acetalization reaction of glycerol were carried out by following the same procedure as stated in General Introduction [Page 47-49].

RESULTS AND DISCUSSION

Characterization of SiW_{11}

Elemental Analysis

The elemental analysis of isolated sodium salt of SiW_{11} exhibited the presence of all expected elements. Table 1 shows the wt% of all the elements obtained by EDS was in good agreement with that of the theoretically calculated ones. These observed values confirm the successful formation of SiW_{11}.

Table 1 Elemental analysis of SiW_{11}

Elements	Theoretical (wt%)	By EDS (wt%)
W	66.3	64.8
Si	0.9	0.88
Na	6.02	6.1
O	26.4	28.7

TGA

The TGA curve of SiW_{11} is shown in Figure 1. The initial weight loss of ~ 5% was observed up to 129 °C corresponding to the desorption of adsorbed water molecules. The second weight loss was observed loss up to 250 °C of 2.0 – 2.3% which may be attributed to the loss of crystalline water molecules. After that, the steady weight loss indicates the decomposition of SiW_{11} species.

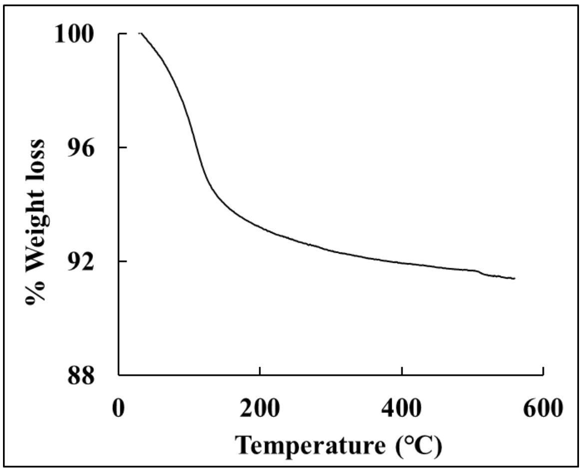

Figure 1 TGA curve of SiW_{11}

The number of water molecules present in SiW_{11} was determined from the above TGA curve by using the following formula,

$$18n = \frac{X\,[M + 18n]}{100}$$

Where, n = number of water molecules, X = % loss from TGA and M = molecular weight of a substance (without crystalline water molecules)

Based on the elemental analysis as well as thermal analysis, the chemical formula of the isolated sodium salt of SiW_{11} was obtained as,

$$Na_8\,[SiW_{11}O_{39}].11H_2O$$

FT-IR

The FT-IR spectra of SiW_{12} and SiW_{11} are shown in Figure 2. SiW_{12} shows the characteristic bands at 985 cm^{-1}, 926 cm^{-1}, 878 cm^{-1}, and 779 cm^{-1} which correspond to W=O_d, Si–O_a, W-O_b-W and W-O_c-W asymmetric stretching vibrations respectively, Where O_a, O_b, O_c, and O_d belong to the oxygen atoms bonded to silicon, bridging to two tungsten (from two different triads for O_b and the same triad for O_c), and to the terminal addenda atom W=O, respectively. In the FT-IR spectra of SiW_{11}, the typical bands appear at 956 cm^{-1} and 887 cm^{-1}, corresponding to W=O_d and Si-O_a stretching vibrations. While two bands were observed here for W- O_b -W at 795 cm^{-1} and 725 cm^{-1}.

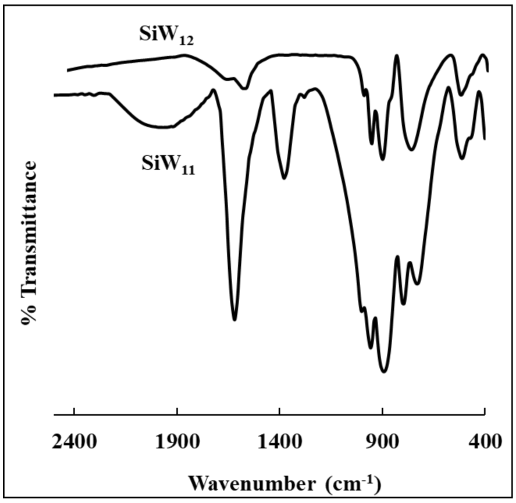

Figure 2 FT-IR spectra of SiW_{11} and SiW_{12}

This splitting in a band may be attributed to the change in symmetry from Td (SiW_{12}) to Cs (SiW_{11}) around the central heteroatom, silicon. These observations are in good agreement with the reported values [11] and thus confirm the formation of SiW_{11}.

^{29}Si MAS NMR

^{29}Si MAS-NMR is a chief technique to know the chemical environment around the silicon nuclei. Figure 3 shows the ^{29}Si MAS-NMR spectrum of SiW_{11}. A single sharp peak at 84.6 ppm was observed, which is in good agreement with the reported value [12]. The single peak confirms the formation of single, un-fragmented species, SiW_{11}.

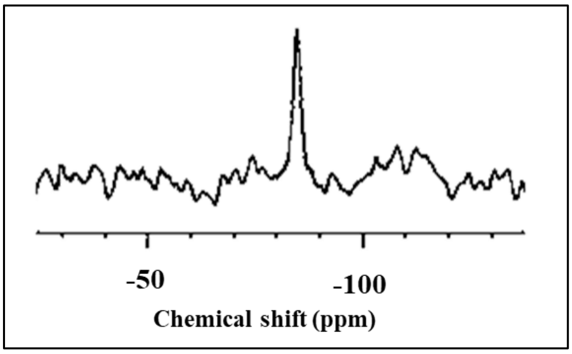

Figure 3 ^{29}Si MAS NMR spectra of SiW_{11}

Characterization of SiW_{11}/nMCM-48

Acidity measurement

The plots of electrode potential as a function of mEq/g of n-butylamine, for nMCM-48 and the catalysts, are shown in Figure 4 and the values for acidic strength as well as sites are depicted in Table 2. nMCM-48 shows moderate acidic nature, owning an acidic strength of 168 mV, with the total acidic sites of 2.4 mEq/g. As the amount of SiW_{11} increases from 10 - 30%, the acidic strength and sites increase significantly from 337 to 476 mV and 2.5 to 3.9 mEq/g respectively. It is a certain indication of successful impregnation of SiW_{11} inside the porous framework. The enhancement is due to the presence of Bronsted acid sites present in SiW_{11}. Nevertheless, only a minor augmentation of acidic strength and sites was observed when the amount was increased to 40% loading. A negligible difference between 30 and 40% loaded catalysts may be ascribed to the saturation or blocking of surface pores of the support. Therefore, here also $(SiW_{11})_3$/nMCM-

48 was considered to be optimum and 30% SiW_{11} was found to be a suitable amount for loading.

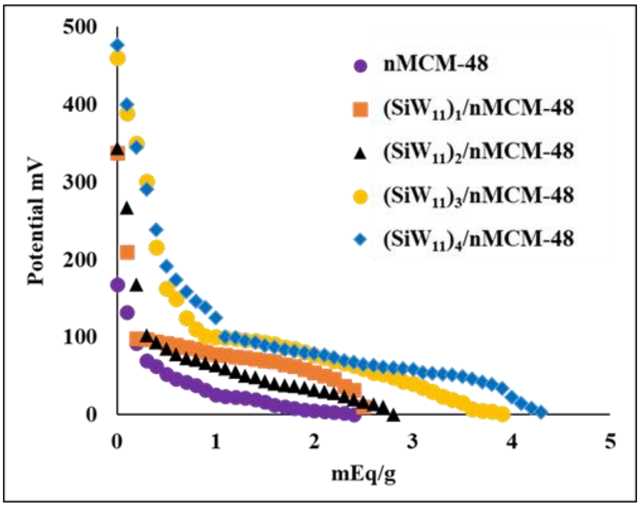

Figure 4 Potentiometric titration curves

Table 2 Acidity measurements of support and catalysts

Materials	Acidic strength (mV)	Types of acidic sites (mEq/g)		Total No. of acidic sites (mEq/g)
		Very strong	Strong	
nMCM-48	168	0.1	2.3	2.4
$(SiW_{11})_1$/nMCM-48	337	0.1	2.4	2.5
$(SiW_{11})_2$/nMCM-48	344	0.3	2.5	2.8
$(SiW_{11})_3$/nMCM-48	460	0.9	3.0	3.9
$(SiW_{11})_4$/nMCM-48	476	1.1	2.2	3.3

BET surface area measurement

The BET surface area and pore measurements of nMCM-48 and catalysts are presented in Table 3. It is observed that when nMCM-48 was impregnated with SiW_{11}, a gradual decrement in the surface area as well as the pore measurements were observed. This change is quite substantial in 10, 20 and 30% loaded catalysts, signifying the interaction and effective impregnation of SiW_{11}. As we increase the amount to 40%, despite a decrease in surface area, there was a negligible change in the pore volume as well as pore diameter. The reason behind this is may be the blocking of sites or surface saturation of support after 30% loading. Thus, considering the said aspects, 30% loading was optimized and its detailed characterization was carried out. For simplicity, the catalyst $(SiW_{11})_3$/nMCM-48 was redesignated as SiW_{11}/nMCM-48.

Table 3 Textural properties of support and catalysts

Materials	BET Surface area (m^2/g)	Pore diameter (Å)	Pore volume (cm^3/g)
nMCM-48	1307	20.8	0.63
$(SiW_{11})_1$/nMCM-48	583	20.5	0.50
$(SiW_{11})_2$/nMCM-48	551	20.2	0.53
$(SiW_{11})_3$/nMCM-48	516	19.1	0.40
$(SiW_{11})_4$/nMCM-48	442	18.0	0.39

The nitrogen adsorption-desorption isotherms of nMCM-48 and SiW_{11}/nMCM-48 are displayed in Figure 5. Generally, Type IV isotherms are given by mesoporous adsorbents. As explained in Part A Chapter 1, nMCM-48 exhibits type IV(b) reversible isotherm without hysteresis loop indicating the smaller width and nano-porous structure. However, it is interesting to note that the in catalyst the type IV(b) isotherm changes to Type IV(a) and hysteresis starts to occur for pores wider than ~ 4 nm, indicating filling of pores via a multilayer formation and capillary condensation. However, it should be noted that the ordered 3D nano-porous structure of support remains intact. This observation can be further explained as, the structure of nMCM-48 is 3D and cubic nano-porous, hypothetically anchoring the lacunary SiW_{11} may lead to cavitation and delayed condensation directing the formation of H4 hysteresis loop. Also, supposedly, the size of SiW_{11} is smaller than that of SiW_{12} and so, after anchoring the widening of pores occurs, which is evident from the pore size distribution [13,14]. Moreover, a decrease in the adsorbed quantity of gas, as compared to nMCM-48, gives the indication of effective filling of pores.

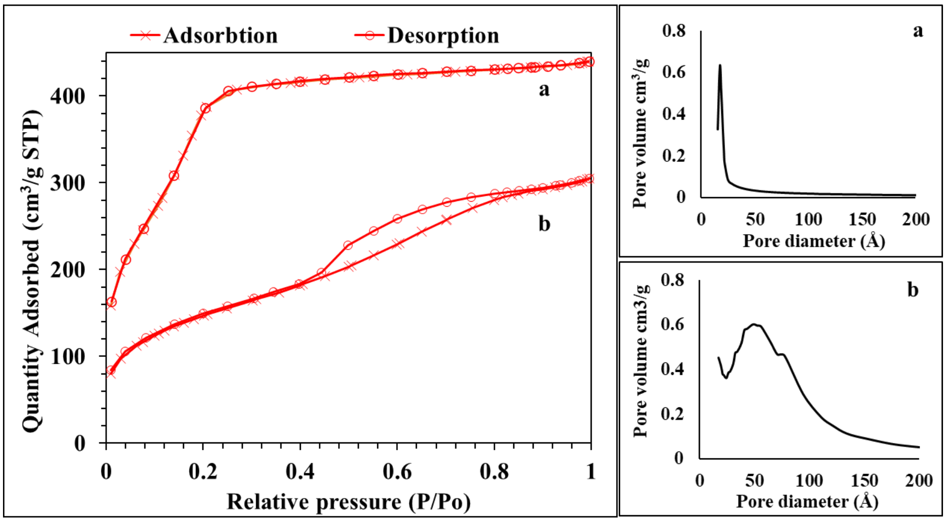

Figure 5 Nitrogen adsorption-desorption isotherms and pore size distribution of a) nMCM-48 and b) SiW_{11}/nMCM-48

Elemental analysis

Elemental analysis by EDS (Figure 6) shows the presence of all expected elements in SiW_{11}/nMCM-48. The obtained value of wt% of W by EDS (Table 4) was found to be similar to the calculated one. This indicates the effective loading of SiW_{11}.

Table 4 Elemental analysis of catalyst

Material	Si (wt%)	O (wt%)	W (wt%)	
			By EDS	Theoretical
SiW_{11}/nMCM-48	59.03	25.68	15.67	15.29

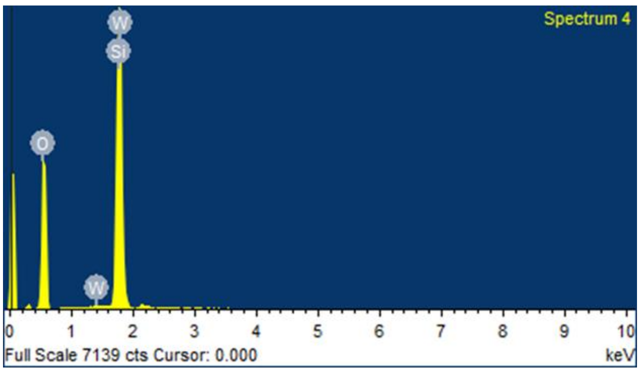

Figure 6 EDS elemental mapping of SiW_{11}/nMCM-48

TGA

The TGA curves for nMCM-48 and SiW_{11}/nMCM-48 are shown in Figure 7. nMCM-48 shows the weight loss in two stages. The initial weight loss of up to 110 °C of 8.9% was observed due to the desorption of absorbed water molecules. The final weight loss of up to 400 °C of <1% was observed because of the condensation of silanol groups present on the surface of support [15]. On further increasing the temperature, no weight loss was observed, which suggests its stability at a higher temperature. From the curves, it is seen that after the impregnation of SiW_{11}, the stability increased as compared to that of the support. For SiW_{11}/nMCM-48, the initial weight loss of 3.92% up to 95 °C corresponds to adsorbed water and the second weight loss up to 150 °C of 0.3% due to the loss of water of crystallization associated with the keggin unit was observed. After that there was no weight loss, indicating the higher thermal stability of the catalyst.

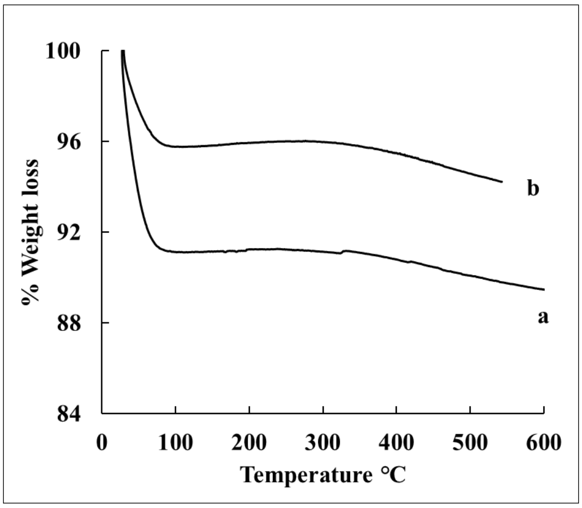

Figure 7 TGA curves of a) nMCM-48 and b) SiW_{11}/nMCM-48

FT-IR

The FT-IR spectra of nMCM-48 and SiW_{11}/nMCM-48 (Figure 8) show two broad bands in the range of 3448 - 3456 cm^{-1} and 1064 -1250 cm^{-1} corresponding to the hydroxyl of silanol groups and Si-O-Si asymmetric stretching vibrations, respectively [16]. In the case of catalyst, the characteristic bands of SiW_{11} (as shown above) at 964 (W-O_d) and 794 (W-O_c-W) were also observed where O_c and O_d are the oxygen atoms bridging two tungsten from the same triad and the terminal oxygen atoms, respectively. The presence of these bands in the fingerprint region, suggests the intact keggin structure even after the impregnation onto nMCM-48. Though, the other bands are not distinctly visible due to their superimposition with the support.

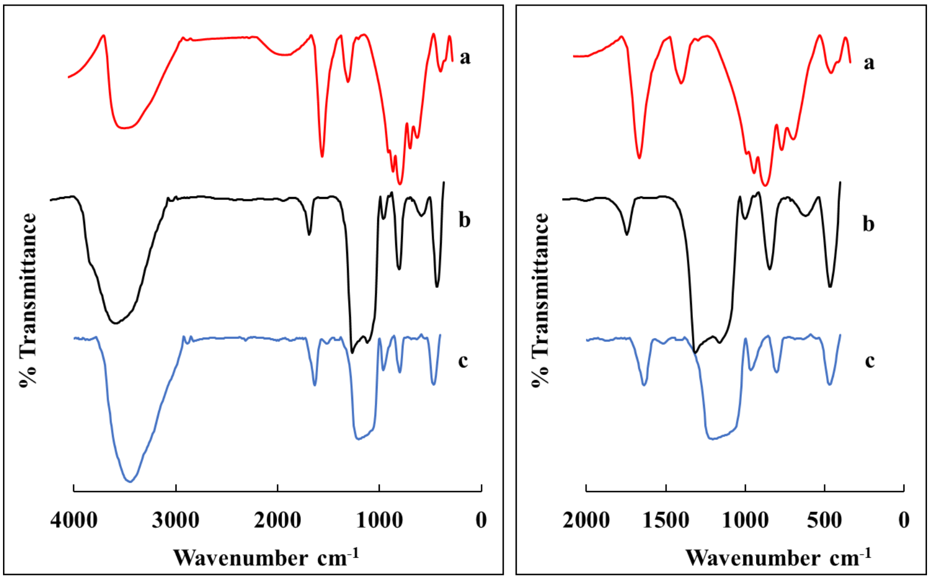

Figure 8 FT-IR spectra of a) SiW_{11}, b) nMCM-48 and c) SiW_{11}/nMCM-48

Powder XRD

The low angle and wide angle powder XRD patterns of nMCM-48 and SiW_{11}/nMCM-48 are shown in Figure 9. The explanation for the XRD pattern of nMCM-48 is given in Part A Chapter 1. In the XRD pattern of catalyst, all the characteristic peaks of nMCM-48 are observed, however, there is a decrease in the intensity of peaks with minor broadening, due to the impregnation of SiW_{11} inside the pores on nMCM-48. Besides, in the wide angle XRD pattern, the crystalline peaks of, SiW_{11} (inset) were not observed, denoting its fine dispersion in the porous framework of nMCM-48 [8]. Thus, from the above observations, it can be concluded that the structure of support remains unchanged even after the impregnation of SiW_{11}.

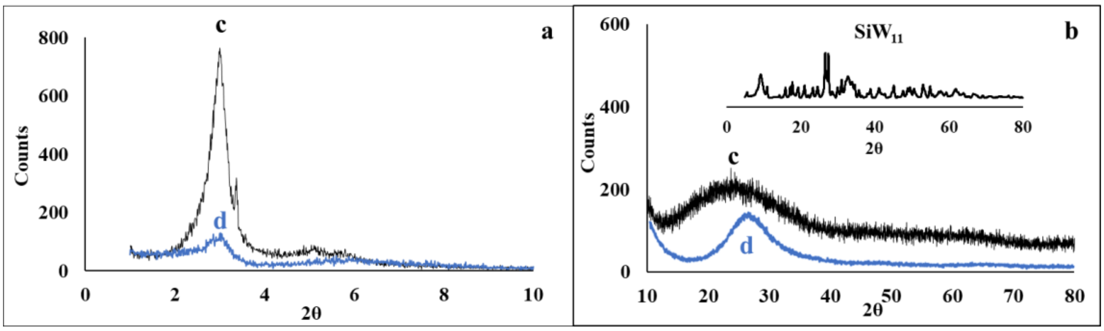

Figure 9 a) Low angle and b) Wide angle XRD patterns of c) nMCM-48 and d) SiW_{11}/nMCM-48, SiW_{11} (Inset)

^{9}Si MAS NMR

The ^{29}Si MAS NMR analysis was carried out to know the chemical interactions between nMCM-48 and SiW_{11}. As mentioned in Part A chapter 1, nMCM-48 (Figure 10a) typically shows a broad peak between -95 and -120 ppm attributing to the three main components Q^2, Q^3 and Q^4, where the notation Q^x indicates the type siloxane linkages [17]. The chemical shift values of SiW_{11}, nMCM-48 and SiW_{11}/nMCM-48 are displayed in Table 5. The peaks corresponding to all the above components were also spotted in the spectra of SiW_{11}/nMCM-48 (Figure 10b). A minor upfield shift in the Q^2 and Q^3 components was observed as compared to that of support. While, it is interesting to note that a major upfield shift was noticed for Q^4 (112.14 ppm). This change may be attributed to the supposition that, nMCM-48 is 3D nano-porous cubic structure, and SiW_{11} is present in the vicinity of adjacent Si atoms. As there is an increase in the electron density (compared to SiW_{12}, SiW_{11} possesses more negative charge), the Si atoms, responsible for giving Q^4 signals, will be more shielded, manifesting the signal in upfield region. Thus, the change in the chemical shift values clearly suggests the presence of strong hydrogen bonding between the SiW_{11} and nMCM-48. Furthermore, a signal corresponding to SiW_{11} also appeared with a minor shift (as compared to bare SiW_{11}) at -79.16 ppm, portraying the unchanged keggin structure.

Table 5 ^{29}Si chemical shifts of nMCM-48 and SiW_{11}/nMCM-48

Materials	Si nuclei ppm (SiW_{11})	Q^2 ppm	Q^3 ppm	Q^4 ppm
nMCM-48	-	-95.51	-103.97	-106.53
SiW_{11}/nMCM-48	-79.16	-97.20	-104	-112.14

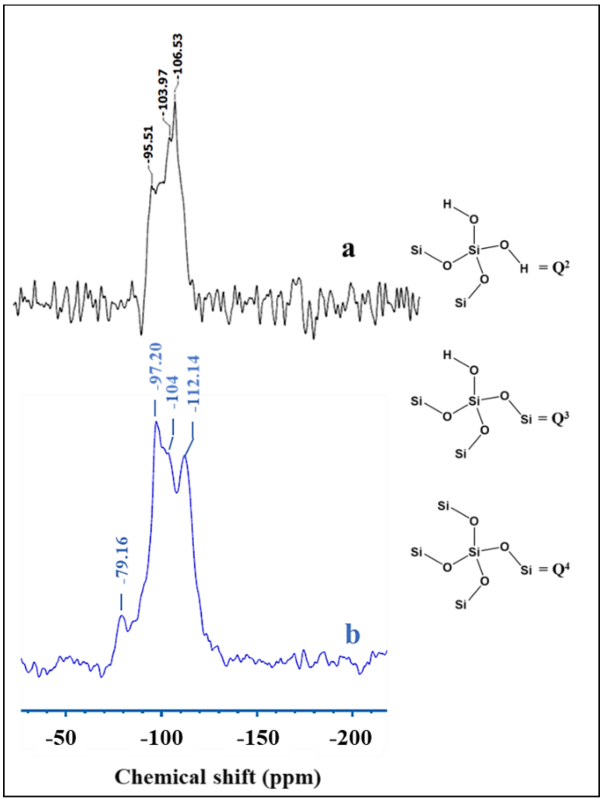

Figure 10 ^{29}Si MAS NMR of a) nMCM-48 and b) SiW_{11}/nMCM-48

TEM

TEM images of nMCM-48 and SiW_{11}/nMCM-48 are shown in Figure 11. As explained earlier in Part A Chapter 1, nMCM-48 shows a regular nano-porous structure with well-ordered pore networks and uniform particle size. Whilst, for SiW_{11}/nMCM-48, widening of the pores was observed which is already explained in detailed by BET textural properties. Also, uniform dispersion of SiW_{11} was observed on the surface as well as inside the nano pores of the support, which was also observed in the XRD analysis. Furthermore, the shape of the particles of nMCM-48 does not show any distortion, indicating its unchanged structure after the impregnation.

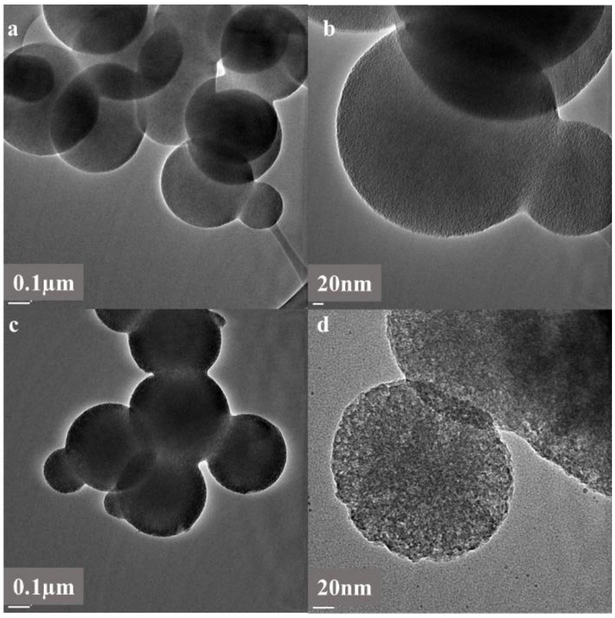

Figure 11 TEM images of a, b) nMCM-48 and c, d) SiW_{11}/nMCM-48

To conclude, the FT-IR analysis confirm the successful formation of mono lacunary species, SiW_{11}. The BET surface area analysis shows successful filling of SiW_{11} inside the pores of nMCM-48, while FT-IR confirms the intact structure of the keggin unit as well as support after impregnation. The Powder XRD fine suggests the dispersion of SiW_{11} and TEM analysis indicates intact morphology of support with widening of pores and uniform dispersion of SiW_{11}. whereas ^{29}Si MAS NMR validates the presence hydrogen bonding between the active species and support.

Catalytic activity

Leaching test

The sustainability of SiW_{11}/nMCM-48 was investigated by carrying out leaching test of the catalyst as stated in General introduction [Page 46]. The absence of formation of heteropoly blue colour indicated that no leaching of SiW_{11} occurred from the hold of nMCM-48 and the catalyst is stable.

a) Esterification of levulinic acid with n-butanol

Similar to the previous chapter, the evaluation of the catalytic activity of SiW_{11}/nMCM-48 for the esterification of levulinic acid with n-butanol as well as its optimization study was carried out by studying all the reaction parameters (% loading of SiW_{11}, mole ratio of levulinic acid to n-butanol, catalyst amount, reaction temperature and time of contact). The parameters were optimized for obtaining the maximum conversion of levulinic acid and selectivity of butyl levulinate.

The required content of active species that imparts the acid sites was varied by keeping experiments in 10 to 40% loading of SiW_{11} and the results are given in Figure 12a. An anticipated increment in the conversion of levulinic acid was observed with an increase in the amount of SiW_{11}. From 10 to 30% loading, the conversion increased gradually from 32% to 49% with 84% as the maximum selectivity of butyl levulinate. This observation can be ascribed to the enrichment of available acid sites on increasing the content of SiW_{11}. But, the trend converses with 40% loading. The conversion declined to 41% at higher concentrations, which may be due to the blocking of catalytic sites or formation of viscous reaction mixture [18]. Henceforth, for further study, 30% loaded catalyst was optimized.

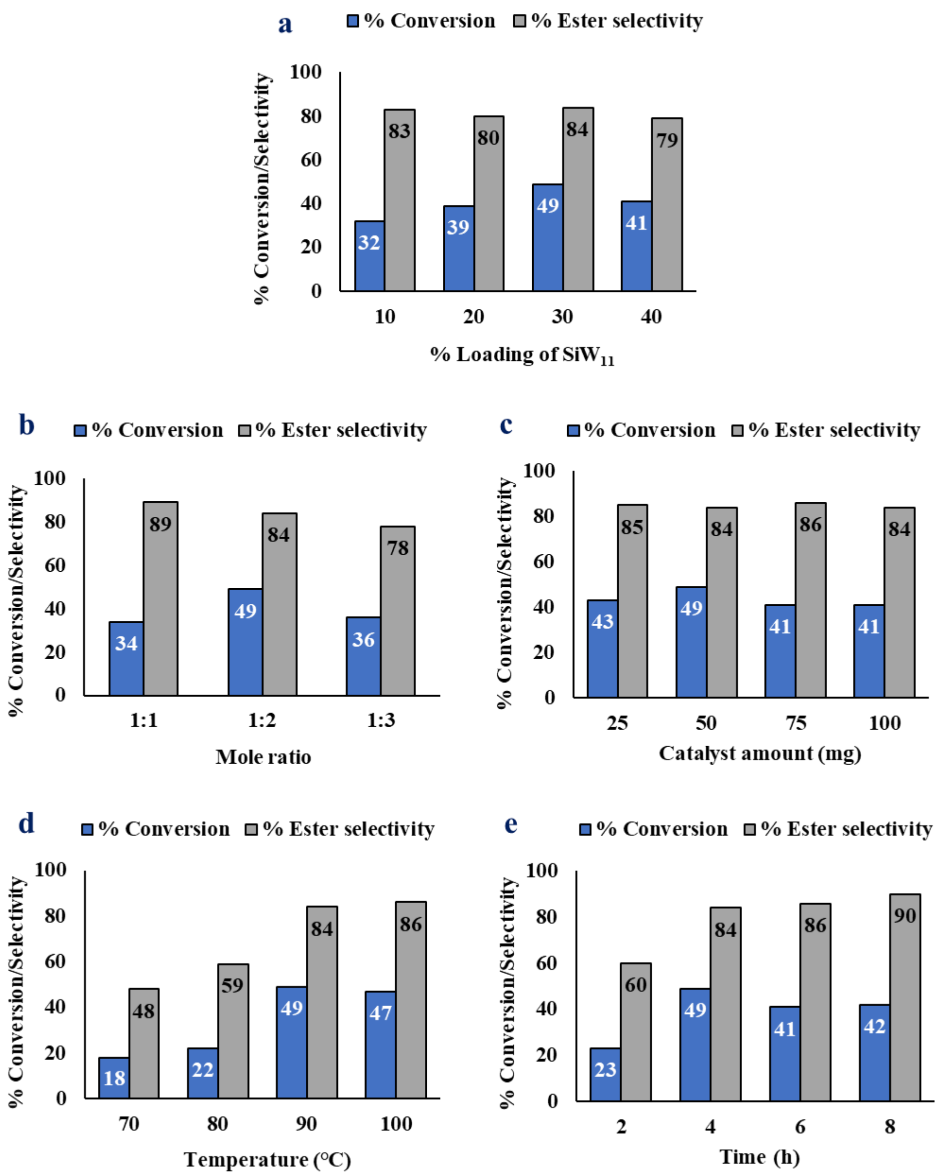

Figure 12 Reaction conditions a) Effect of % loading of SiW_{11}. Mole ratio: 1:2; Catalyst amount: 50 mg; Temperature: 90 °C; Time: 4 h, b) Effect of mole ratio. Catalyst amount 50 mg; Temperature 90 °C; Time 4h, c) Effect of catalyst amount. Mole ratio 1:2; Temperature 90 °C; Time 4h, d) Effect of temperature. Mole ratio 1:2; Catalyst amount 50 mg; Time 4h, e) Effect of time. Mole ratio 1:2; Catalyst amount 50 mg; Temperature 90 °C.

The effect of the mole ratio was studied by carrying out experiments from 1:1 to 1:3 and the obtained results are shown in Figure 12b. In a 1:2 ratio, maximum conversion of levulinic acid, 49% with 84% selectivity towards butyl levulinate was achieved. The esterification process is prone to reverse hydrolysis when water is present in the medium, hence an excess of alcohol is required to shift the equilibrium in a forward direction. Despite increasing the ratio to 1:3, the conversion reduced to 36%, probably due to the dilution of the acidic reaction medium with excess alcohol. A similar trend was seen with SiW_{12}/nMCM-48. Therefore, 1:2 was found to be the optimum molar ratio for SiW_{11}/nMCM-48 also.

One more important parameter is the catalyst amount. Reactions using 25 to 100 mg of catalyst were carried out and the results are presented in Figure 12c. The reaction proceeds to give 43% conversion in 25 mg to 49% in 50 mg with no change in the selectivity of ester. More is the catalyst amount; more is the number of available catalytic sites and favours the conversion of acid into ester. But beyond 50 mg, in higher catalyst amount i.e., 75 mg and 100 mg, the conversion slightly drops and may attain equilibrium. This impact is due to the increase in the mass density of the reaction mixture with the more solid catalyst which may block some of the active catalytic sites. It hinders the easy transport of reactants and products on the surface and inside the porous network. Thus, the 50 mg catalyst amount was optimized.

To study the influence of temperature, the reactions were carried out at 70, 80, 90 and 100 °C (Figure 12d). As observed, with the rise in temperature from 70 to 90 °C, the conversion increases gradually from 18 to 49% and the selectivity of butyl levulinate nearly doubled from 48 to 84%. Temperature provides thermal energy to the reactant molecules and increases collisions between them [19]. Thus, at elevated temperatures, the reaction becomes faster and yields good conversion. At 100 °C, no significant change in the conversion was noted. Hence, looking at the maximum conversion as well as selectivity, 90 °C temperature was optimized.

The contact time of reactants also plays a central role in reversible reactions. To study the effect of time, the reaction was screened from 2 to 8 h (Figure 12e). When the reaction was allowed to continue from 2 to 4 h, here also, the conversion increased twofold from 23 to 49%. However, on prolonging the reaction for 6 and 8 h, the conversion drops which may be due to the reversible nature of reaction. As a result, 4 h was optimized as an appropriate reaction time.

From the above study, the optimized reaction parameters are, mole ratio (levulinic acid/n-butanol) 1:2; catalyst amount 50 mg (active amount of SiW_{11} 11.54 mg), temperature 90 °C; time 4 h and maximum conversion of 49% with 84% ester selectivity was achieved with an excellent TON of 1300 and TOF of 325 h^{-1}.

b) Esterification of succinic acid with n-butanol

The versatile nature of SiW_{11}/nMCM-48 was evaluated for esterification of succinic acid with n-butanol and a detailed optimization study was carried out by investigating different reaction parameters with the focus on obtaining the maximum conversion of acid and selectivity towards dibutyl succinate (diester), similar to the previous chapter.

The feasibility of the reaction was checked first with different % loading amounts of SiW_{11}. An increase in the number of catalytic sites with SiW_{11} loading favoured the conversion of acid into esters. From the results (Figure 13a) it was observed that here also, 30% loaded catalyst gave maximum conversion (77%) of succinic acid with 42% selectivity towards dibutyl succinate (Diester). Hence, it was optimized and selected for further studies.

To assess the effect of the mole ratio, experiments with varying ratio from 1:1 to 1:4 was carried out (Figure 13b). Increasing molar ratio assisted the acid conversion as well as the formation of diester. A maximum of 82% conversion was achieved in the 1:4 mole ratio, however, the selectivity towards the diester decreased to 37% as compared to that obtained in the 1:3 mole ratio (42%). Also, an excess of alcohol may cause the dilution of the reaction mixture and hinders the second esterification. Hence, the 1:3 mole ratio was considered to be optimum for the reaction.

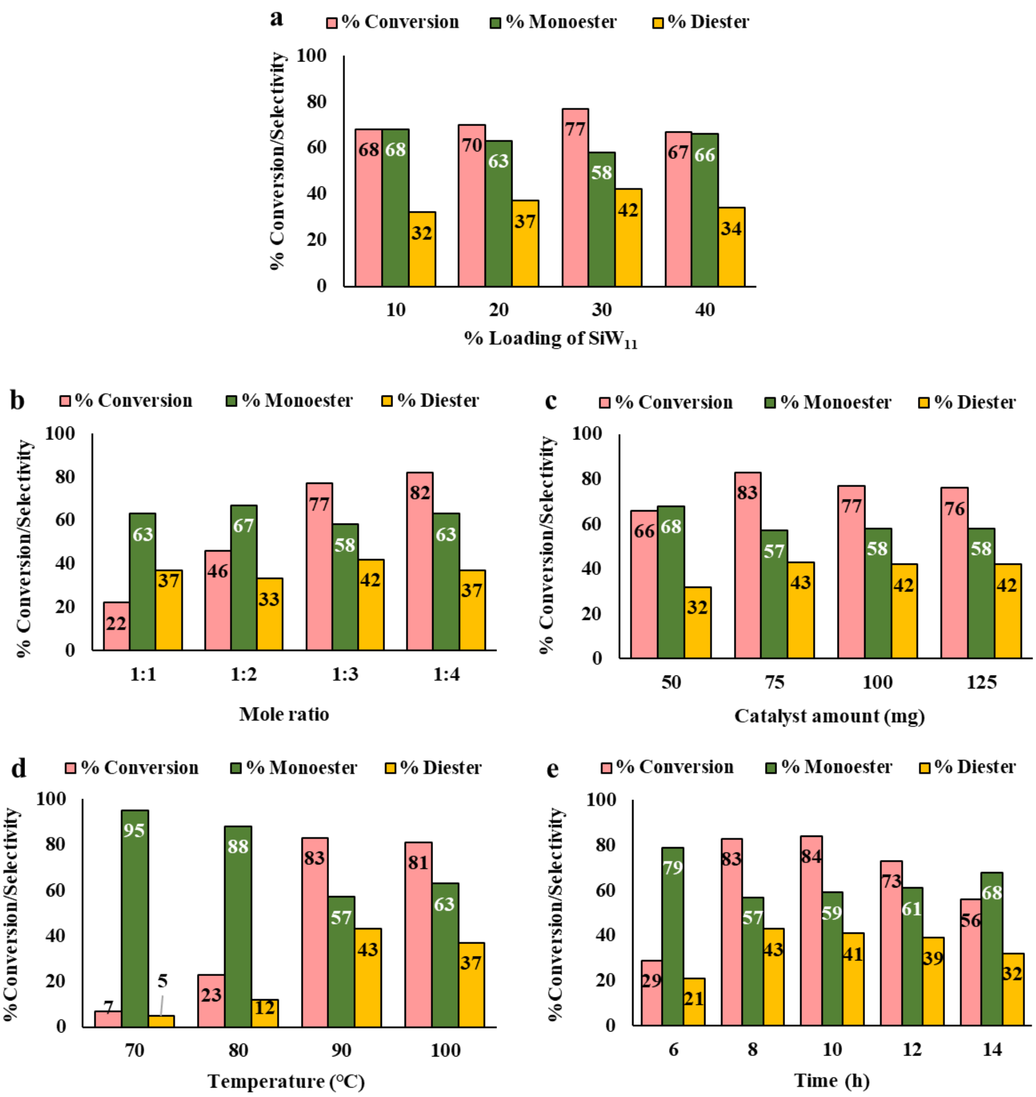

Figure 13 Reaction conditions a) Effect of % loading of SiW_{11}. Mole ratio: 1:3; Catalyst amount: 100 mg; Temperature: 90 °C; Time: 8 h, b) Effect of mole ratio. Catalyst amount 100 mg; Temperature 90 °C; Time 8h, c) Effect of catalyst amount. Mole ratio 1:3; Temperature 90 °C; Time 8h, d) Effect of temperature. Mole ratio 1:3; Catalyst amount 75 mg; Time 8h, e) Effect of time. Mole ratio 1:3; Catalyst amount 75 mg; Temperature 90 °C

The influence of catalyst amount was investigated by keeping reactions in 50, 75, 100 and 125 mg catalyst (Figure 13c). With the upsurge in catalyst amount, the conversion of acid is expected to increase as the number of acid sites also increases. Nonetheless, the maximum conversion, as well as selectivity of the diester, was achieved in 75 mg of catalyst amount. Beyond it, the conversion of acid was reduced which may be attributed to the increase in overall solid mass density at a higher catalyst amount. Therefore, 75 mg is an appropriate catalyst amount for this transformation.

Likewise, the effect of reaction temperature and time was studied. The results are shown in Figure 13d and Figure 13e. Both the parameters are vital for the reaction to proceed successfully and to yield the selectivity of the desired product. At elevated temperatures, the conversion increases tremendously to four-fold at 90 °C. As the reaction is endothermic, higher temperature promotes molecular collisions as well as diesterification. At the same temperature, the conversion hiked in 8 h and beyond that prolonging the reaction time did not significantly contribute to the conversion rate as well as selectivity. Hence, 90 °C temperature and 8 h reaction time were found to be optimum.

The optimized reaction conditions with SiW_{11}/nMCM-48 for maximum conversion of succinic acid (83%) and selectivity of diester (43%) are, mole ratio 1:3; catalyst amount 75 mg (active amount of SiW_{11} 17.3 mg); temperature 90 °C and time 8 h. The TON and TOF were found to be 1466 and 183 h^{-1} respectively.

c) Acetalization of glycerol with furfural

The catalytic efficiency of SiW_{11}/nMCM-48 for acetalization of glycerol with furfural was also checked and a detailed optimization study was carried out using similar reaction parameters as mentioned in the previous chapter. The formation of acetals as well as their selectivity is governed by the acidic character of a catalyst. Here also, the focus was narrowed to obtain the maximum glycerol conversion and selectivity towards the dioxane derivative. The scheme of the reaction can be referred from Part A Chapter 1.

Initially, the experiments were performed to select the best % loading amount of SiW_{11} for this transformation, so the reactions were carried out using 10-40% loaded catalyst and the results are tabulated in Figure 14a. The conversion of glycerol steadily increased with the % loading of SiW_{11}, as the amount of acid sites increased. The acidic sites activate the furfural and aids in reaction progress. More is the catalyst loading; more is the activation of reactant molecules and greater is the conversion. This trend with SiW_{11}/nMCM-48 was quite slow as compared to that with SiW_{12}/nMCM-48. The highest % conversion of glycerol, 27% was found in the 30% loading of SiW_{11}. Therefore, analogous to the previous study, a 30% loaded catalyst was found to be optimum.

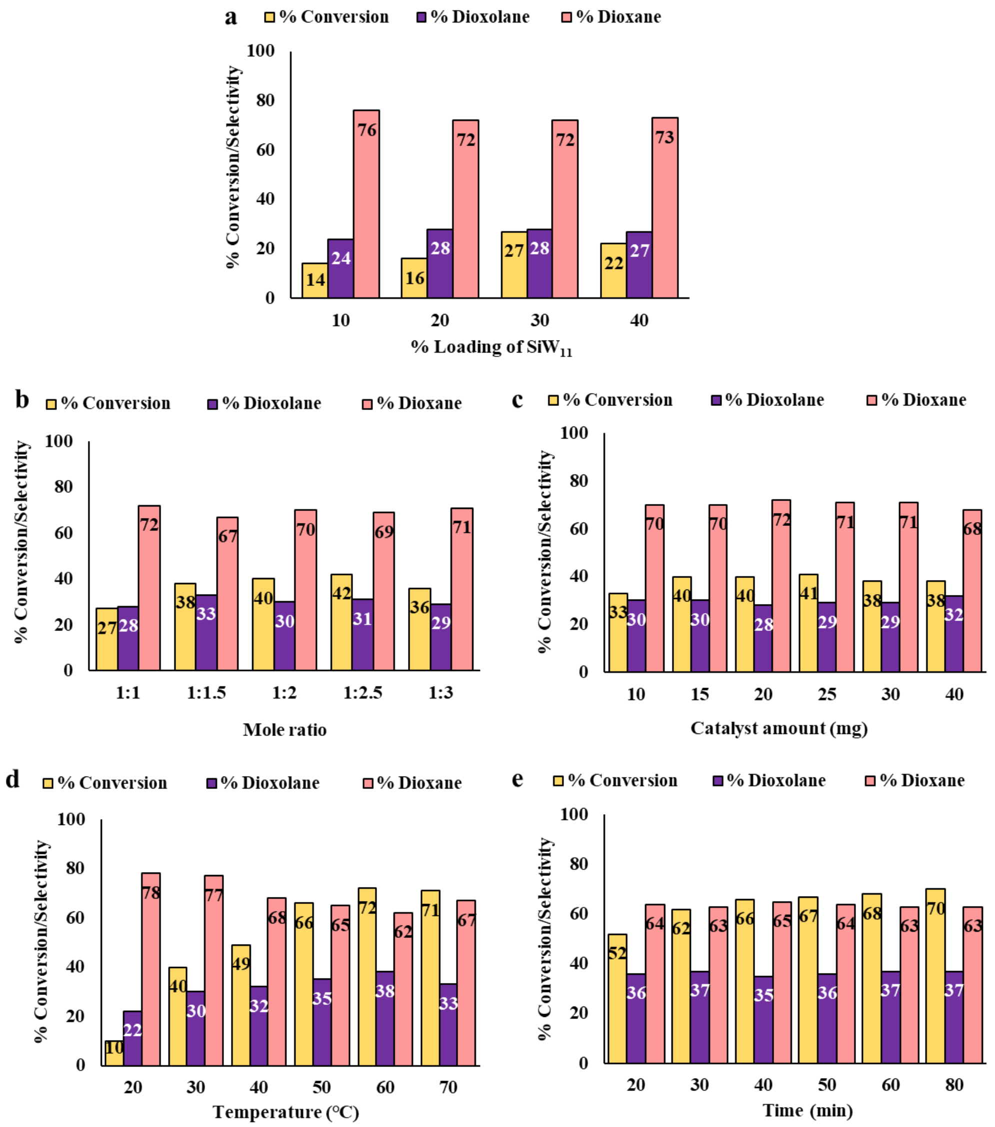

Figure 14 Reaction conditions a) Effect of % loading of SiW_{11}. Mole ratio 1:1; Catalyst amount 15 mg; Temperature 30 °C; Time 40 min b) Effect of mole ratio. Catalyst amount 15 mg; Temperature 30 °C; Time 40 min, c) Effect of catalyst amount. Mole ratio 1:2; Temperature 30 °C; Time 40 min, d) Effect of temperature. Mole ratio 1:2; Catalyst amount 15 mg; Time 40 min, e) Effect of time. Mole ratio 1:2; Catalyst amount 15 mg; Temperature 50 °C.

The molar concentration of glycerol and furfural has a certain effect on the conversion rate, which is evident from Figure 14b. When both the reactants were taken in equal stoichiometry, only 27% conversion was obtained. Up to 1:2.5 molar ratio, the conversion increased gradually and beyond that in 1:3, it slightly dropped. An excess of furfural may block the catalytic sites and the overcrowding of reactants on the catalyst surface hampers the activation of furfural molecules, resulting in lower conversion. However, no significant change in the conversion was observed in the 1:2 and 1:2.5 molar ratios. Also, an irregular trend in the selectivity of 1,3-dioxane was seen. Thus, considering the said aspects, a 1:2 mole ratio of glycerol to furfural was considered to be optimum.

The influence on the reaction was studied in different catalyst amounts and the results are shown in Figure 14c. It is assumed that with more catalyst amount, there will be more amount of available catalytic sites/acid sites which will be responsible for carrying out the reaction. A maximum conversion of 40% and 70% selectivity of 1,3-dioxane was achieved in 15 mg of catalyst. A further increase in amount did not cause any change. Henceforth, 15 mg was found to be adequate for the reaction.

The initial rate and the final conversion of the reaction may be affected by the temperature. Figure 14d shows the influence of SiW_{11}/nMCM-48 catalyzed reactions at 20 to 70 °C. An increase in temperature leads to higher conversion up to 50 °C. Beyond that, the graph shows a steady plateau and 66% conversion and 65% towards 1,3-dioxane was achieved in 50 °C. Thus, 50 °C temperature was enough to promote the reaction.

To study the effect of reaction time, experiments were performed for 20 to 80 mins (Figure 14e). From 20 to 80 min the % conversion of glycerol increased from 52 to 70% with no significant effect on the selectivity of 1,3-dioxane. With time, the reaction progresses well as the contact time between the reactants allowed more collisions and conversion into product molecules. But, prolonged reaction time after 40 mins does not show a substantial change in the activity. Thus, 40 min was optimized as the required time for the reaction.

The optimized conditions for glycerol acetalization with SiW_{11}/nMCM-48 are mole ratio 1:2, catalyst amount 15 mg (active amount of SiW_{11} 3.46 mg), temperature 50 °C, time 40 mins. Maximum conversion of 66% and 65% selectivity towards 1,3-dioxane, with TON and TOF of 5827 and 8697 h^{-1}, respectively.

All the obtained products were analysed by gas chromatography and the chromatographs are shown in Figure 15, Figure 16 and Figure 17.

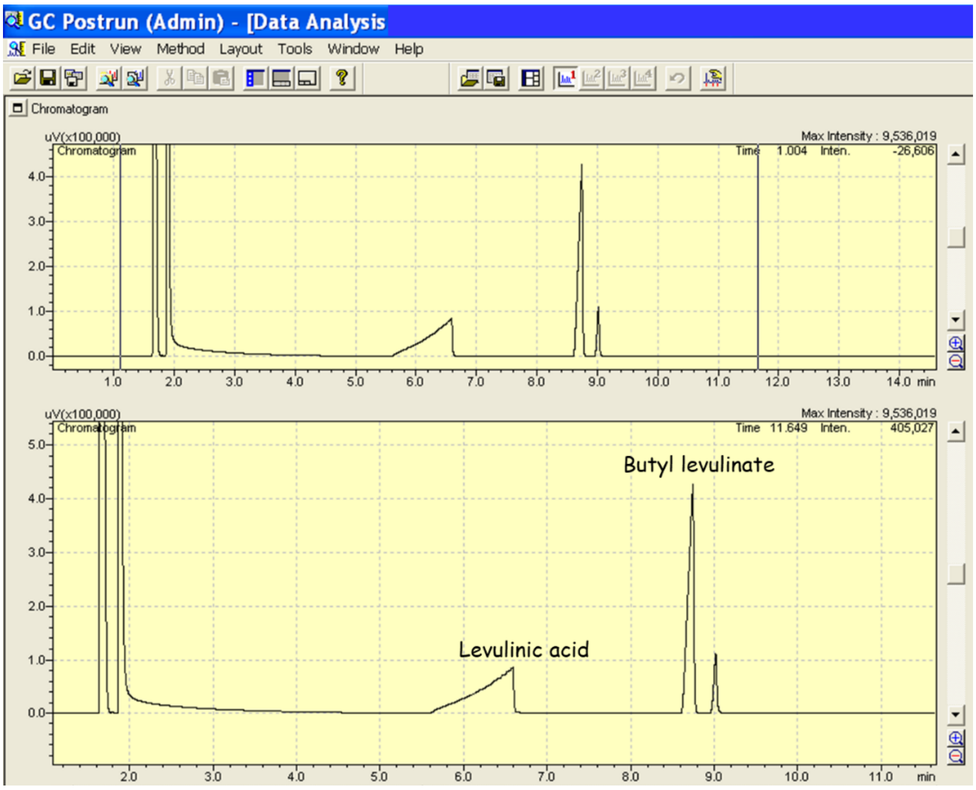

Figure 15 Gas chromatograph of levulinic acid esterification

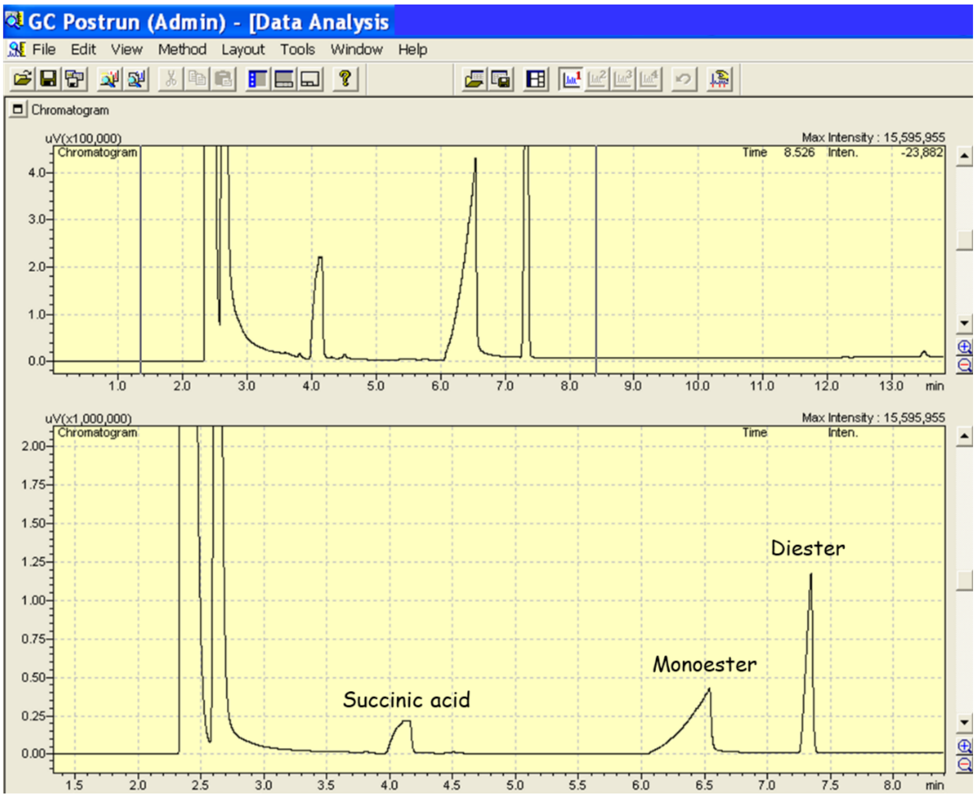

Figure 16 Gas chromatograph of succinic acid esterification

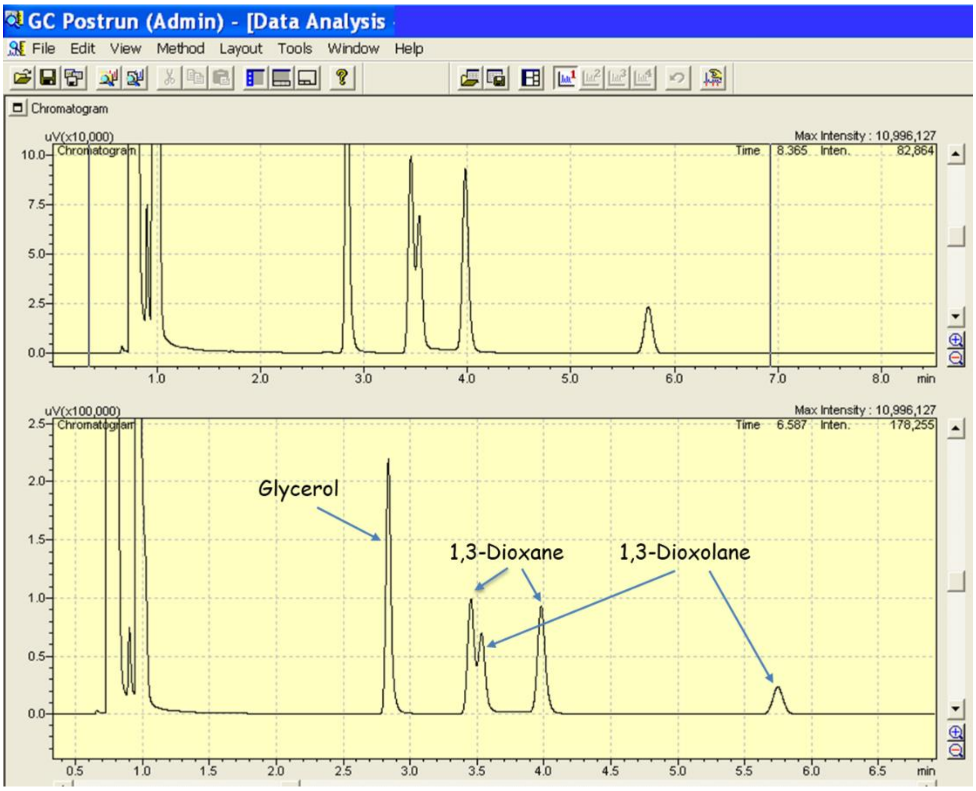

Figure 17 Gas chromatograph of glycerol acetalization

Control experiments

The control experiments with SiW_{11} and nMCM-48 were carried out for the above transformations in their respective optimized conditions and the results are shown in Table 6. Analogous to the observations of the previous chapter, when the reactions were carried out with nMCM-48 alone, the conversion of both the acids was found to be less as compared to that with bare SiW_{11}. However, it shows some activity towards the conversion of glycerol. With the catalyst, appreciable conversion and selectivity towards respective desired products was achieved, reflecting that SiW_{11} is active and responsible species for the catalytic activity. The Bronsted acidity present in SiW_{11} plays chief role in promoting the esterification as well as acetalization reactions. Thus, the combined properties of SiW_{11}, as an active species and nMCM-48 as support forms a truly heterogeneous catalyst.

Table 6 Control experiments

Materials	% Conversion/ %Selectivity of desired product*		
	^{a}Levulinic acid esterification	^{b}Succinic acid esterification	^{c}Glycerol acetalization
nMCM-48	24/100	52/27	32/60
SiW_{11}	38/79	58/27	23/73
SiW_{11}/nMCM-48	49/84	83/43	66/65

Reaction conditions mole ratio ^{a}1:2, ^{b}1:3, ^{c}1:2; catalyst amount nMCM-48 ^{a}38.46 mg, ^{b}57.7 mg, ^{c}11.54 mg; SiW_{11} ^{a}11.54 mg, ^{b}17.3 mg, ^{c}3.46 mg; SiW_{11}/nMCM-48 ^{a}50 mg, ^{b}75 mg, ^{c}15 mg; temperature ^{a}90 °C, ^{b}90 °C, ^{c}50 °C; time ^{a}4 h, ^{b}8 h, ^{c}40 min.
*Selectivity of ^{a}Butyl levulinate, ^{b}Diester (Dibutyl succinate) and ^{c}1,3-dioxane

Regeneration and recycling studies

The catalyst used in the first cycle was regenerated by the method reported in Part A chapter 1. A regenerated catalyst was employed for subsequent catalytic cycles for all the reactions and the results are displayed in Figure 18. The graphs show the consistent activity of the catalyst till 3 cycles for all the transformations. In the case of levulinic acid esterification, after the second cycle, the conversion as well as selectivity drops. While for succinic acid esterification and glycerol acetalization, reliable conversion as well selectivity towards desired products were obtained till 3 cycles and slightly drops in 4th one. This decrease may be attributed to the loss of catalyst amount during regeneration process. However, one can also reuse the catalyst for multiple cycles until the complete deactivation of catalyst, depending on the chemist's choice. Thus, recycling experiments determine that the catalyst is stable to use for multiple cycles, validating its sustainable nature.

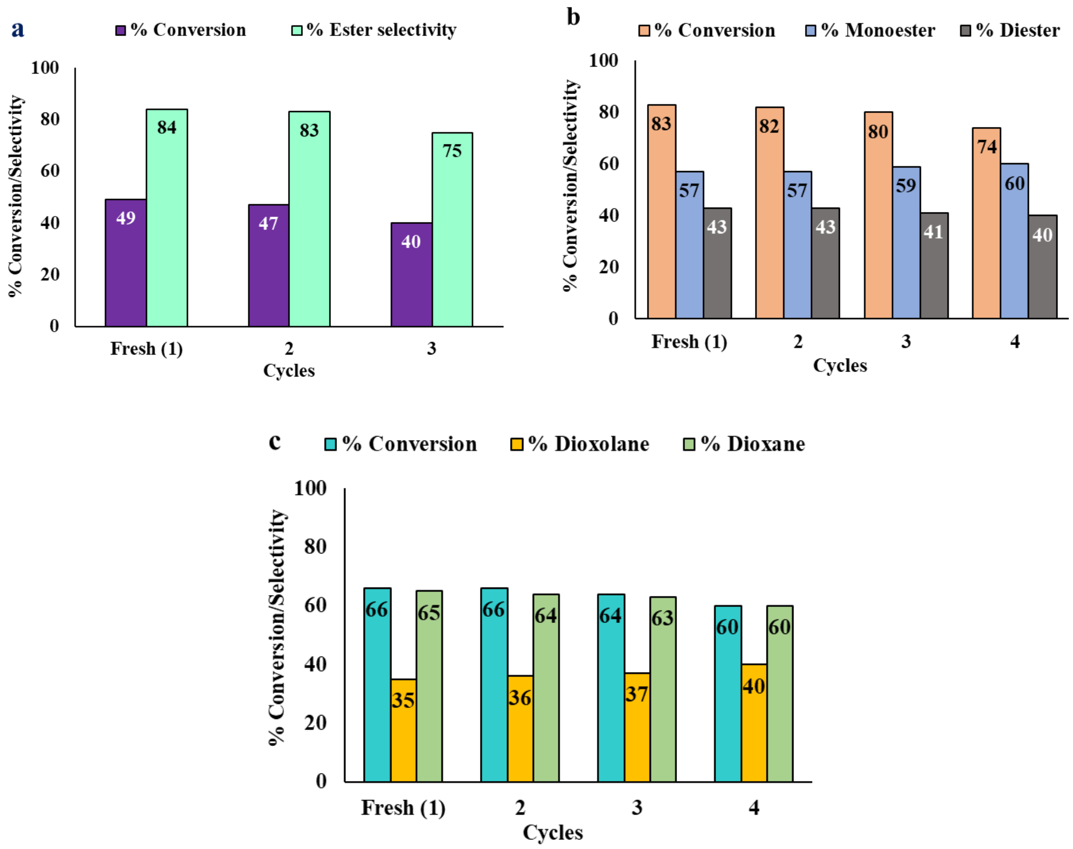

Figure 18 Recycling experiments for a) levulinic acid esterification, b) succinic acid esterification and c) glycerol acetalization

Characterization of regenerated catalyst

The regenerated SiW_{11}/nMCM-48 was characterized by acidity measurement, BET surface area and FT-IR analysis. As observed from the table, the obtained acidic strength and sites of the regenerated catalyst are almost similar to that of the fresh one, signifying unchanged acidic character. The nitrogen adsorption-desorption isotherms (Figure 19a and b) of regenerated catalyst are found to be similar to that of the fresh one, suggesting the intact structure of the catalyst. However, a negligible change in surface area (Table 7) may be attributed to the sticking of reactants/products after reaction on the catalyst surface. Similarly, in FT-IR spectra (Figure 19c) all the characteristic bands of the catalyst, as explained in the characterization section (for fresh catalyst), are present in the regenerated one, confirming the intact structure of the keggin unit. Thus, the above observation supports the impervious catalytic behaviour for more than one cycle.

Table 7 Acidity measurements and BET surface area of fresh and regenerated catalyst

Catalysts	Acidic strength (mV)	Total Acidic Sites (mEqui/g)	BET surface area (m^2/g)
Fresh	460	3.9	516
Regenerated	453	3.6	520

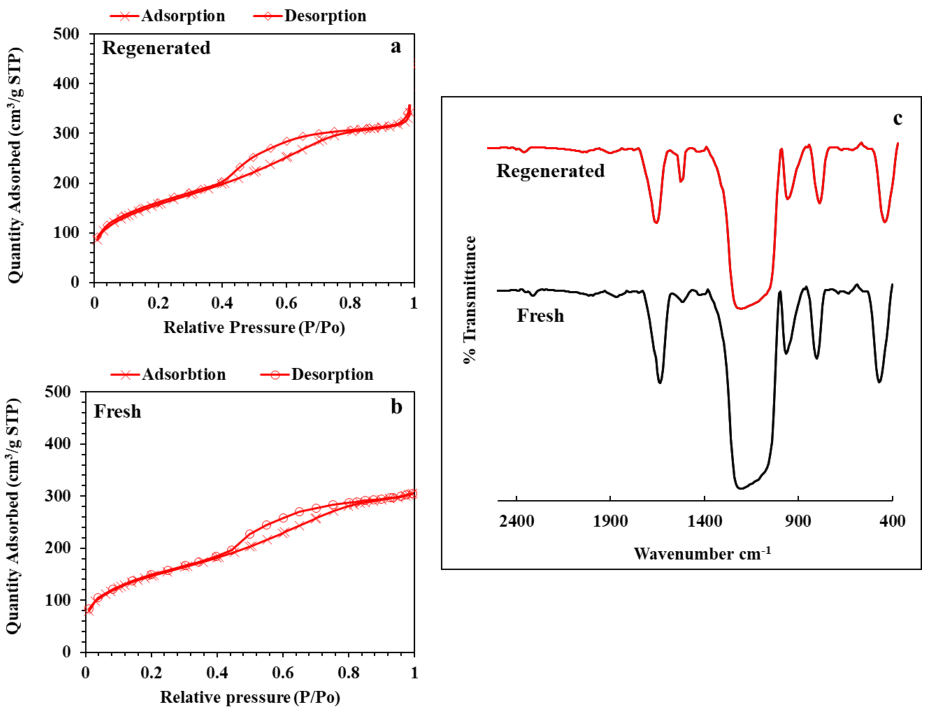

Figure 19 Nitrogen adsorption-desorption isotherms of a) regenerated and b) fresh catalyst and c) FT-IR spectra of regenerated and fresh catalyst

Activity of catalyst for esterification reactions under identical conditions

The activity of the catalyst for esterification reaction was checked by carrying out the experiments for both acids in optimized conditions of levulinic acid esterification. From the data (Table 8) it was observed that under the identical conditions, the succinic acid gets converted to its esters by only 14% while levulinic acid shows 49% conversion. It indicates that the esterification of levulinic acid is faster as compared to that of succinic acid. This observation was found similar to previous catalyst.

Table 8 Esterification reactions under identical conditions

Conditions / Reactions	In optimized conditions of levulinic acid esterification*	
	% Conversion of acid	% Selectivity of desired ester
Levulinic acid esterification	49	84
Succinic acid esterification	14	08 (Diester)

*Reaction conditions mole ratio 1:2; catalyst amount 50 mg; temperature 90 °C; time 4 h

Kinetic study: Determination of activation energy

The activation energy for all three transformations in SiW_{11}/nMCM-48 was determined by carrying out experiments at different temperatures and time intervals, by keeping other parameters constant as in an optimized condition of reaction.

a) Activation energy for esterification of levulinic acid with n-butanol

A graph of 1/(a-x) Vs time was plotted (Figure 20), from the results obtained by carrying out experiments for esterification of levulinic acid with n-butanol using a 1:2 mole ratio for different time intervals (2, 4 and 6 h) at 90 °C. The graph shows a linear relationship of reaction corresponding to time and confirms its second-order dependence.

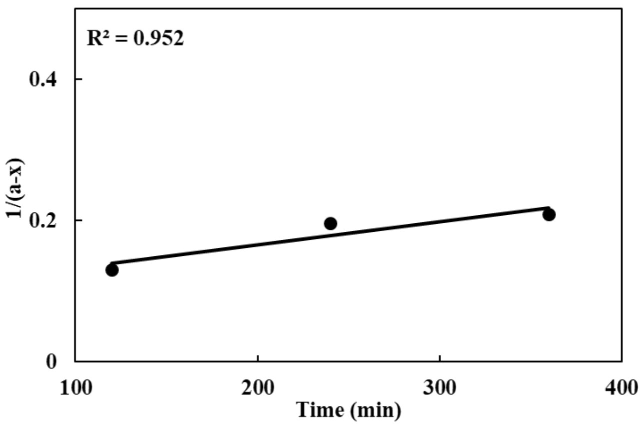

Figure 20 Plot of 1/(a-x) Vs Time for levulinic acid esterification

By keeping the reactions at different time intervals, the rate constant at each temperature (343 to 373 K) was calculated (Table 9). With an increase in temperature, the rate of reaction also increases. The graph of ln k Vs 1/T was plotted (Figure 21) and from the slope of the graph, the activation energy was calculated using the Arrhenius equation and found to be 29 kJ/mol.

Table 9 Rate constants (k M^{-1} min^{-1}) and activation energy (Ea)

Temperature (K)	Rate constant k (M^{-1} min^{-1})	Activation energy Ea (kJ/mol)
343	4.0×10^{-4}	29
353	5.0×10^{-4}	
363	7.0×10^{-4}	
373	9.0×10^{-4}	

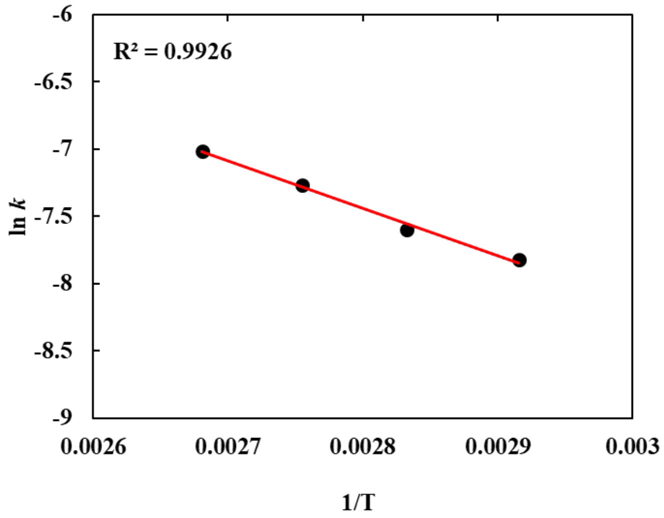

Figure 21 Plot of ln *k* Vs 1/T for levulinic acid esterification

b) Activation energy for esterification of succinic acid with n-butanol

The kinetic experiments for the esterification of succinic acid and n-butanol were carried out in a 1:3 molar ratio for different time intervals (6, 8 and 10 h) at 90 °C. The plot of 1/(a-x) Vs time (Figure 22) was plotted from the obtained results and it demonstrates a linear relationship with respect to time confirming the second-order dependence of reaction.

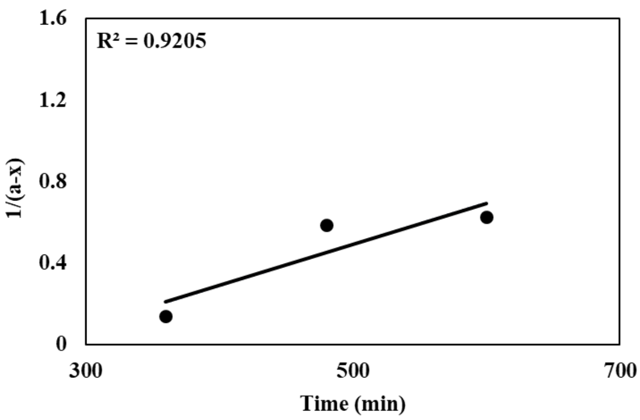

Figure 22 Plot of 1/(a-x) Vs Time for succinic acid esterification

In order to determine the rate constants at different temperatures, the reactions were performed at 343 to 373 K and the results are shown in Table 10. Here also, the rate of reaction increases with temperature. From the results, the graph of ln *k* Vs 1/T was plotted to determine the activation energy (Figure 23). Using the Arrhenius equation from the slope of the graph the activation energy was found to be 75 kJ/mol. Relative to SiW_{12}/nMCM-48, the activation energy here with mono lacunary catalyst, SiW_{11}/nMCM-48 is quite higher. However, it may be anticipated that the catalyst may lower the activation energy if the reaction would be carried out at an elevated temperature, i.e., above 373 or 383 K. Here, considering the green parameters, the kinetic experiments have not been tried at elevated temperatures

Table 10 Rate constants (*k* M^{-1} min^{-1}) and activation energy (Ea)

Temperature (K)	Rate constant *k* (M^{-1} min^{-1})	Activation energy Ea (kJ/mol)
343	2.0×10^{-4}	
353	3.0×10^{-4}	75
363	1.0×10^{-3}	
373	1.4×10^{-3}	

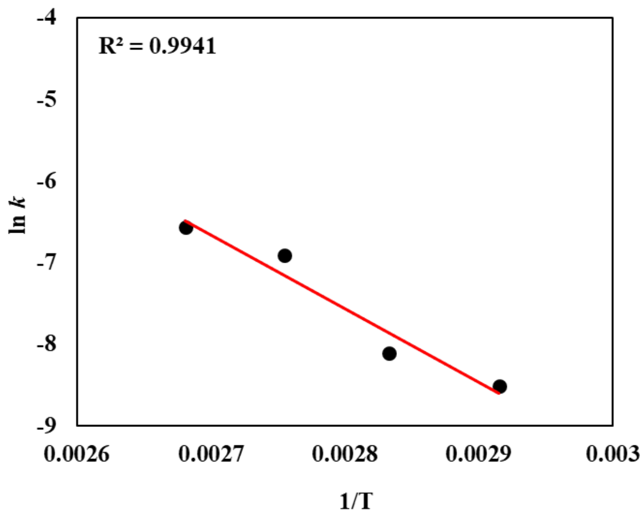

Figure 23 Plot of ln *k* Vs 1/T for succinic acid esterification

c) Activation energy for acetalization of glycerol with furfural

The results obtained in optimized conditions for acetalization of glycerol with furfural in different time intervals (20, 40 and 60 min) at 50 °C were used to plot the graph of 1/(a-x) Vs time. As shown in Figure 24, the graph shows a linear relationship with respect to time, verifying the second-order dependence of reaction.

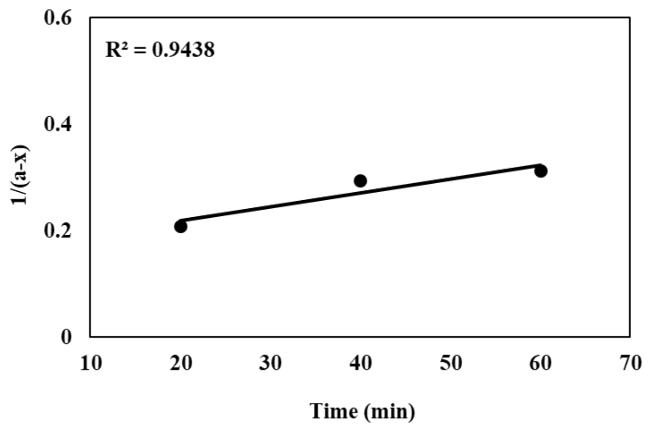

Figure 24 Plot of 1/(a-x) Vs Time for glycerol acetalization

To determine the rate constants at different temperatures (303 to 333 K), reactions were carried out at different time intervals and the obtained results are mentioned in Table 11. Expectedly, the rate constants increase linearly with temperature. From these obtained rate constants, the graph of ln *k* versus 1/T was plotted (Figure 25) and the activation energy was calculated using the Arrhenius equation from the slope of the graph. The activation energy with SiW_{11}/nMCM-48 was found to be 65 kJ/mol.

Table 11 Rate constants (k M^{-1} min^{-1}) and activation energy (Ea)

Temperature (K)	Rate constant k (M^{-1} min^{-1})	Activation energy Ea (kJ/mol)
303	9.0×10^{-4}	65
313	1.80×10^{-3}	
323	6.20×10^{-3}	
333	7.80×10^{-3}	

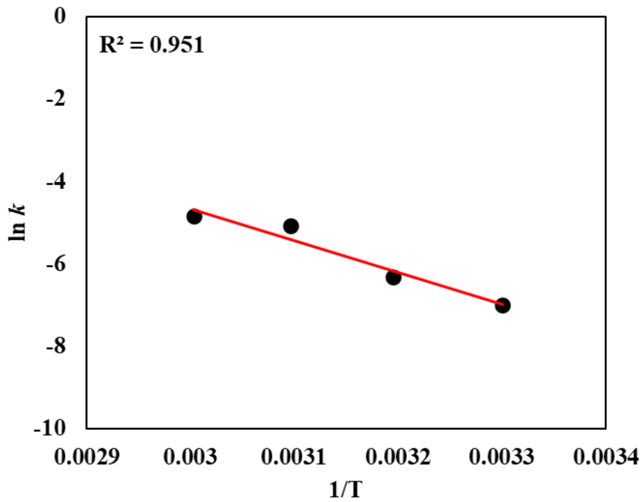

Figure 25 Plot of ln *k* Vs 1/T for glycerol acetalization

An observation similar to the previous chapter was found here also. The activation energy for all the reactions is exceeding 25 kJ/mol, which indicates that in SiW_{11}/nMCM-48, the reactions follow the kinetic regime.

Furthermore, the activation energy for succinic acid esterification with the catalyst was quite high as compared to that of levulinic acid esterification. The explanation for this observation remains the same as given in previous chapter, that more energy is required to carry out esterification of a diacid as compared to mono carboxylic acid and therefore, the activation for esterification of levulinic acid is relatively less.

Plausible mechanism

For all three catalytic transformations using SiW_{11}/nMCM-48, we are expecting the same mechanism as explained in Part A Chapter 1 for SiW_{12}/nMCM-48. Hence detailed explanation is not included here.

CONCLUSION

- A successful synthesis of a heterogeneous catalyst comprising SiW_{11} and nMCM-48 was achieved. The detailed characterization confirms the efficacious filling of nanopores of nMCM-48 with SiW_{11} without any alteration in structure of either one.
- The promising catalytic activity of the catalyst was reflected in the appreciable conversion of bioplatform molecules, levulinic acid (49%), succinic acid (83%) and glycerol (66%).
- Admirable TON/TOF for esterification reactions (1300/325 for levulinic acid and 1466/183 for succinic acid) as well as acetalization reaction (5827/8697 for glycerol) was achieved at ambient reaction temperatures.
- The activation energy for all transformations were found to exceed 25 kJ/mol (29 kJ/mol for levulinic acid esterification, 75 kJ/mol for succinic acid esterification, and 65 kJ for glycerol acetalization).

REFERENCES

1. M. T. Pope and A. Müller, Angewandte Chemie International Edition in English 30, 34 (1991).
2. D. Li, Y. Guo, C. Hu, L. Mao, and E. Wang, Appl Catal A Gen 235, 11 (2002).
3. Y. Guo, Y. Yang, C. Hu, C. Guo, E. Wang, Y. Zou, and S. Feng, J Mater Chem 12, 3046 (2002).
4. X. Luo and C. Yang, Phys Chem Chem Phys 13, 7892 (2011).
5. C. M. Granadeiro, A. D. S. Barbosa, P. Silva, F. A. A. Paz, V. K. Saini, J. Pires, B. de Castro, S. S. Balula, and L. Cunha-Silva, Appl Catal A Gen 453, 316 (2013).
6. X. Dong, C. Yu, D. Wang, Y. Zhang, P. Wu, H. Hu, and G. Xue, Mater Res Bull 85, 152 (2017).
7. S. Pathan and A. Patel, J Coord Chem 63, 4041 (2010).
8. A. Patel and N. Narkhede, Catal Sci Technol 3, 3317 (2013).
9. N. Narkhede and A. Patel, RSC Adv 4, 64379 (2014).
10. A. Patel, N. Narkhede, and A. Patel, Catal Survfrom Asia 23, 257 (2019).
11. T. Okuhara, N. Mizuno, and M. Misono, in edited by D. D. Eley, W. O. Haag, and B. B. T.-A. in C. Gates (Academic Press, 1996), pp. 113–252.
12. L. C. Moura, J. G. Eon, S. Caldarelli, and S. Paul, Ann Magn Reson 4, 86 (2005).
13. M. Thommes, K. Kaneko, A. v. Neimark, J. P. Olivier, F. Rodriguez-Reinoso, J. Rouquerol, and K. S. W. Sing, Pure Appl Chem 87, 1051 (2015).
14. K. A. Cychosz and M. Thommes, Engineering 4, 559 (2018).
15. S. Singh and A. Patel, J Clean Prod 72, 46 (2014).
16. Y. Zhang and S. Yang, J Wuhan Univ Technol Mater Mater Sci Ed 23, 346 (2008).
17. W. Zhang and T. J. Pinnavaia, Catal Letters 38, 261 (1996).
18. K. C. Badgujar, V. C. Badgujar, and B. M. Bhanage, Fuel Process Technol 197, 106213 (2020).
19. Y. Chen, X. Zhang, M. Dong, Y. Wu, G. Zheng, J. Huang, X. Guan, and X. Zheng, J Taiwan Inst Chem Eng 61, 147 (2016).